

Low-plasma and high-temperature PECVD grown silicon-rich  $\text{SiO}_x$  film with enhanced carrier tunneling and light emission

This article has been downloaded from IOPscience. Please scroll down to see the full text article.

2007 Nanotechnology 18 395202

(<http://iopscience.iop.org/0957-4484/18/39/395202>)

The Table of Contents and more related content is available

Download details:

IP Address: 140.112.113.225

The article was downloaded on 11/02/2009 at 03:46

Please note that terms and conditions apply.

# Low-plasma and high-temperature PECVD grown silicon-rich $\text{SiO}_x$ film with enhanced carrier tunneling and light emission

Gong-Ru Lin<sup>1</sup>, Chun-Jung Lin and Cheng-Tao Lin

Graduate Institute of Photonics and Optoelectronics, Department of Electrical Engineering, National Taiwan University, No. 1 Roosevelt Road Section 4, Taipei 106, Taiwan, Republic of China

E-mail: [gmlin@ntu.edu.tw](mailto:gmlin@ntu.edu.tw)

Received 1 May 2007, in final form 19 July 2007

Published 4 September 2007

Online at [stacks.iop.org/Nano/18/395202](http://stacks.iop.org/Nano/18/395202)

## Abstract

Low-plasma and high-temperature chemical vapor deposition of Si-rich  $\text{SiO}_x$  for concurrently enhancing the carrier tunneling and light emission efficiency is investigated. The O/Si composition ratio of the  $\text{SiO}_x$  film significantly decreases from 2 to 1.2 as the substrate temperature increases from 200 to 400 °C, corresponding to the enhanced precipitation of Si nanocrystals in the Si-rich  $\text{SiO}_x$ . In comparison with stoichiometric  $\text{SiO}_2$ , the Si-L<sub>2,3</sub> transition induced kinetic energy loss of the primary electron transmitted through the Si-rich  $\text{SiO}_x$  sample grown at 400 °C is red-shifted by 5 eV. The strongest Si nanocrystal related photoluminescence (PL) can be obtained from the Si-rich  $\text{SiO}_x$  film prepared at a threshold plasma power of 30 W and substrate temperature of 400 °C. In low-plasma and high-temperature deposited samples, the threshold Fowler–Nordheim (F–N) tunneling field and the indium tin oxide (ITO)- $\text{SiO}_x$  junction potential barrier height of ITO/ $\text{SiO}_x$ /p-Si/Al metal-oxide-semiconductor light emitting diodes (MOSLEDs) are concurrently reduced due to the increasing density of Si nanocrystals precipitated within the  $\text{SiO}_x$  matrix. A thermal activation energy of 0.8 eV was observed for initiating the F–N tunneling process in the MOSLEDs. The electroluminescence (EL) intensity and efficiency of the MOSLEDs are improved by at least 10 dB due to the oxygen deficient plasma enhanced chemical vapor deposition (PECVD) of Si-rich  $\text{SiO}_x$  at low plasma power and high temperatures.

(Some figures in this article are in colour only in the electronic version)

## 1. Introduction

The research interests in all silicon (Si)-based light-emitting diodes (LEDs) for next-generation Si photonic integrated-circuits (ICs) have recently been stimulated due to the observation of efficient light emission and optical gain [1] in plasma enhanced chemical vapor deposition (PECVD) grown Si-rich silicon dioxide ( $\text{SiO}_x$ ,  $x < 2$ ) films containing

Si nanocrystals (Si nanocrystals). PECVD deposition of  $\text{SiO}_x$ ,  $\text{SiN}_x$ , or  $\text{SiO}_x\text{N}_y$  film at an extraordinary recipe of the mixed gas source containing nitrous oxide ( $\text{N}_2\text{O}$ ), ammonia ( $\text{NH}_3$ ), and monosilane ( $\text{SiH}_4$ ) diluted by nitrogen or hydrogen gas has been treated as the best candidate for the host material of the synthesized Si nanocrystals. It was concluded from the traditional PECVD process that the high radio-frequency plasma power and high substrate temperature benefit from growing stoichiometric  $\text{SiO}_2$ , since both the

<sup>1</sup> Author to whom any correspondence should be addressed.

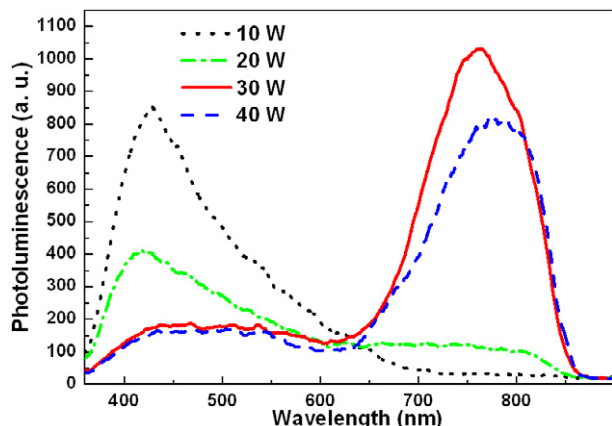


**Figure 1.** PL spectra of PECVD-grown  $\text{SiO}_x$  films deposited at a substrate temperature of  $350^\circ\text{C}$  and different plasma powers of 10, 20, 30, and 40 W.

decomposition and the adsorption rates of Si and oxygen atoms are simultaneously optimized. However, an extremely high plasma power not only suppresses Si-rich  $\text{SiO}_x$  formation but also initiates a surface bombardment to degrade the structural and electrical performances [2–5]. Alternatively, the low-plasma-power PECVD synthesis of  $\text{SiO}_x$  film was considered due to the small dissociation energy of the monosilane as compared to the nitrous oxide [6, 7], which eventually leads to a more pronounced Si adsorption process under a relatively low oxygen decomposition environment. That is, the deposition of excess Si atoms in  $\text{SiO}_x$  film can be enhanced by effectively suppressing the oxygen decomposition at a threshold plasma power. Such a specific PECVD growth of Si-rich  $\text{SiO}_x$  film strictly relies on the control on Si substrate temperature and detuning of the fluence ratio of the  $\text{SiH}_4/\text{N}_2\text{O}$  fluence ratio. By increasing the Si substrate temperature during PECVD growth, we investigate the change in Si/O composition ratio, the Si–Si binding energy, and the effective electron mass of the deposited Si-rich  $\text{SiO}_x$  film. The effects of oxygen deficiency on the density of the post-annealing synthesized Si nanocrystals, and to the electrical and optical properties of the Si-rich  $\text{SiO}_x$  film based metal-oxide-semiconductor light emitting diode (MOSLED) are analysed. The metal-oxide barrier height, the electroluminescence (EL) spectrum and power, and the quantum efficiency of the MOSLED made on the Si-rich  $\text{SiO}_x$  film prepared at different deposition temperatures are compared.

## 2. Experiments

Under a threshold plasma power of 30 W, the Si-rich  $\text{SiO}_x$  films were grown on p-type Si(100) substrate in a PECVD system at a chamber pressure of 60 mTorr, in which  $\text{SiH}_4$  and  $\text{N}_2\text{O}$  fluences were set as 20 and 120 sccm. The threshold power is defined as the smallest plasma power in the PECVD chamber required to decompose the  $\text{SiH}_4$  and  $\text{N}_2\text{O}$  gases and to synthesize the Si-rich  $\text{SiO}_x$  film with Si nanocrystals after annealing. The thicknesses of  $\text{SiO}_x$  films are  $240 \pm 20$  nm by controlling the deposition time at substrate temperature ranging from 200 to  $400^\circ\text{C}$ . A post-annealing process was

performed in a quartz furnace with flowing  $\text{N}_2$  at  $1100^\circ\text{C}$  for 60 min. The composition of the  $\text{SiO}_x$  films grown at different substrate temperatures are analysed from Rutherford backscattering spectrometry (RBS) analysis. RBS analysis at a detecting angle of  $170^\circ$  under 2 MeV  $\text{He}^+$ -ion bombardment was performed, and a commercial software ‘Ramp’ was used to calculate the O/Si composition ratio of the  $\text{SiO}_x$  film. The formation of Si nanocrystals in the low-plasma-power PECVD-grown  $\text{SiO}_x$  at different deposition temperatures was analysed by high-resolution transmission electron microscopy (HRTEM), and the kinetic energy loss of a transmitted primary electron due to the transition of electrons at  $2\text{P}_{1/2}$  and  $2\text{P}_{3/2}$  orbits in Si atoms (denoted as Si- $L_{2,3}$ ) is characterized by electron energy loss spectroscopy (EELS) [8]. To perform the EL diagnosis, an indium tin oxide (ITO)/ $\text{SiO}_x$ /p-Si/Al MOSLED with a contact diameter of 0.8 mm was made. The EL power–current characteristics are analysed by using a laser diode current source (Keithley, SMU-236) in conjunction with an optical power meter and a Si photodiode based integrator sphere (ILX Lightwave 6100 + 6708B).

## 3. Results and discussion

By growing  $\text{SiO}_x$  film under threshold plasma power, we investigate the deposition-temperature dependent evolution on the Si/O composition ratio of an Si-rich  $\text{SiO}_x$  film and the binding energy of electrons at the  $L_{2,3}$  orbits of an Si atom in Si-rich  $\text{SiO}_x$ . The threshold power condition is confirmed from the photoluminescence (PL) analyses of the  $\text{SiO}_x$  films grown at the same substrate temperature and different plasma powers, as shown in figure 1. The  $\text{SiO}_x$  film furnace-annealed at  $1100^\circ\text{C}$  for 60 min exhibits an Si-nanocrystal-dependent near-infrared photoluminescence (PL) spectrum ranging between 670 and 850 nm. The normalized PL intensity ( $\text{count nm}^{-1}$ ) increases by six times as the deposition temperature rises from 200 to  $400^\circ\text{C}$ . Apparently, it is observed on the annealed PECVD-grown Si-rich  $\text{SiO}_x$  film that the Si nanocrystal related PL at near-infrared region can only be observed from the sample deposited at a plasma larger than 30 W. In contrast, a lot of oxygen related defects such as a weak-oxygen-bond, neutral oxygen vacancy (NOV), and ionized oxygen ( $\text{O}_2^-$ ) centers [9, 10] were observed in the PECVD-grown  $\text{SiO}_x$  films deposited at plasma power below 30 W, contributing to the significant PL components in the blue-green region. The maximum PL intensity at a wavelength of 760 nm from the sample deposited at 30 W is higher than that deposited at 10 W by 20 times. Furthermore, the near-infrared PL intensity from the sample deposited at 40 W is slightly lower than that deposited at 30 W as the higher plasma power condition concurrently facilitates the decomposition of  $\text{SiH}_4$  and  $\text{N}_2\text{O}$  as well as the stoichiometric  $\text{SiO}_2$  synthesis. Therefore, the Si density of the PECVD-grown Si-rich  $\text{SiO}_x$  film deposited at 40 W is also smaller than that deposited at 30 W. The RBS analysed curve of the  $\text{SiO}_x$  film grown at a deposition temperature of  $350^\circ\text{C}$  is shown in figure 2. The RBS signals of elements Si and O is determined at corresponding energies of 1.147 and 742.0 keV, respectively. As a result, the O/Si composition ratio is decreased from 2 to 1.2 as the substrate temperature increases from 200 to  $400^\circ\text{C}$ . The RBS analysis shows that the stoichiometry of the PECVD-grown  $\text{SiO}_2$  film

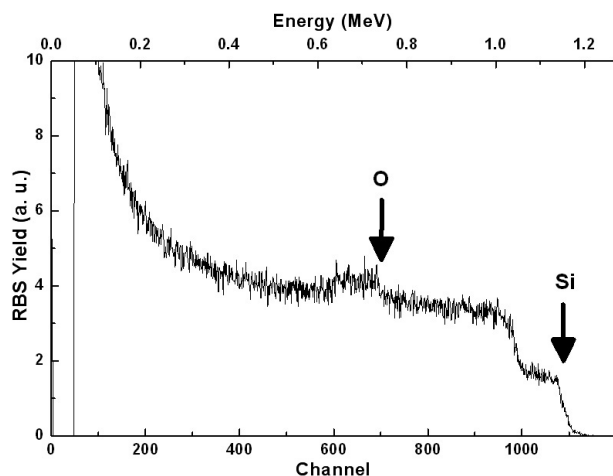


**Figure 2.** RBS spectrum of PECVD-grown  $\text{SiO}_x$  film at a substrate temperature of  $350^\circ\text{C}$  and plasma power of 30 W.

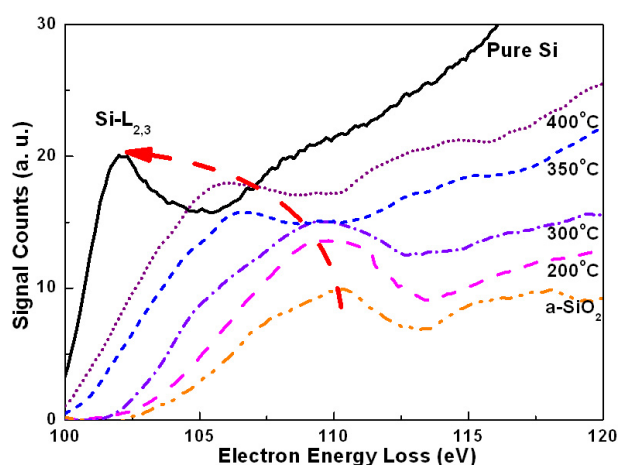


**Figure 3.** The electron energy loss spectra of pure Si, a- $\text{SiO}_2$ , and Si-rich  $\text{SiO}_x$  samples grown at different deposition temperatures.

degrades significantly as the deposition temperature increases to  $300^\circ\text{C}$  or higher. As the substrate temperature increases from  $200$  to  $400^\circ\text{C}$  during PECVD growth, the decreasing O/Si composition ratio correlates well with the enhanced precipitation of Si nanocrystals in the Si-rich  $\text{SiO}_x$ .

Due to the induced transition of the internal electrons at  $2P_{1/2}$  and  $2P_{3/2}$  orbits in an Si atom (denoted as Si- $L_{2,3}$ ), the kinetic energy loss spectrum of a transmitted primary electron can be obtained from EELS analysis. It is also observed from EELS analysis that the EELS peaks for  $\text{SiO}_x$  grown at a threshold plasma power of 30 W are slightly red-shifted from 110 to 106 eV as the deposition temperatures rises from  $200$  to  $400^\circ\text{C}$  (see figure 3). In comparison with the Si- $L_{2,3}$  transition related EELS peak linewidth for standard Si [11], we found that the corresponding spectral linewidth is gradually reduced with increasing deposition temperature. In contrast, the Si- $L_{2,3}$  transition related EELS peak intensity of the PECVD-grown  $\text{SiO}_2$  is greatly attenuated with a broadened spectral linewidth due to its amorphous phase. Figure 4 summarizes that the composition of the PECVD-grown  $\text{SiO}_x$  film deposited at plasma power  $>30$  W

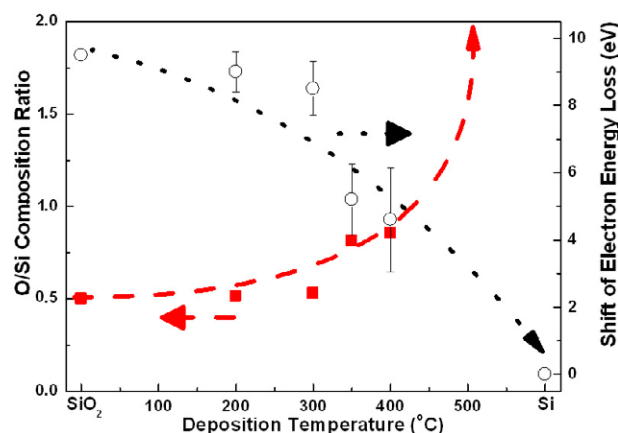


**Figure 4.** The EELS shift of binding energy for the Si- $L_{2,3}$  electron in  $\text{SiO}_x$  and the Si/O composition ratio as a function of deposition temperature.

is more stoichiometric than that deposited at plasma power below 30 W. The determined shift of the EELS peak energy as compared to the Si substrate is significantly reduced with an enlarged oxygen deficiency in the annealed Si-rich  $\text{SiO}_x$ . There is a critical PECVD deposition recipe for the optimized growth of Si-rich  $\text{SiO}_x$  film with maximum Si/O composition ratio. Such a growth condition helps to differentiate the decomposition of Si and O atoms from  $\text{SiH}_4$  and  $\text{N}_2\text{O}$  gases, providing an oxygen deficient environment during the  $\text{SiO}_x$  film deposition procedure. After precipitating the Si nanocrystals within the annealed  $\text{SiO}_x$ , a lower energy loss of the primary electron from the Si- $L_{2,3}$  transition induced by the Si-O ionic bond becomes less pronounced than that by the Si-Si covalent bond due to the relaxation of binding energy for Si- $L_{2,3}$  electrons. This is mainly attributed to the increasing quantity of Si-Si bonds as compared to the Si-O bonds. By increasing substrate temperature from  $200$  to  $400^\circ\text{C}$ , the decreasing O/Si composition ratio correlates well with the decreasing primary electron kinetic energy loss derived from the binding energy of Si- $L_{2,3}$  electrons, which is due to the increasing excess Si atom density as well as the enhanced precipitation of Si nanocrystals in the  $\text{SiO}_x$  deposited at higher substrate temperatures. The lower EELS peak energy and narrower spectral linewidth are strong evidences of the existence of highly concentrated Si nanocrystals buried in the high-temperature grown Si-rich  $\text{SiO}_x$ . The changes in gradient of the EELS peak energy, peak intensity and spectral linewidth become significant at higher deposition temperatures, which confirms the increasing density of Si nanocrystals with increasing deposition temperature.

The EL of the Si-rich  $\text{SiO}_x$  MOSLED is based on the electron-hole recombination in the Si nanocrystals, in which the electron and hole pairs come from the tunneling through ITO- $\text{SiO}_x$  and Si- $\text{SiO}_x$  barriers. The Fowler-Nordheim (F-N) tunneling effect that occurred in the MOSLED sample enhances the carriers dropped into Si nanocrystals [12-14]. A band diagram of the positively biased ITO/ $\text{SiO}_x$ /p-Si/Al MOSLED for explaining the F-N tunneling effect enhanced carrier transport behavior and Si nanocrystal luminescence is shown in figure 5. Unlike the Poole-Frenkel and

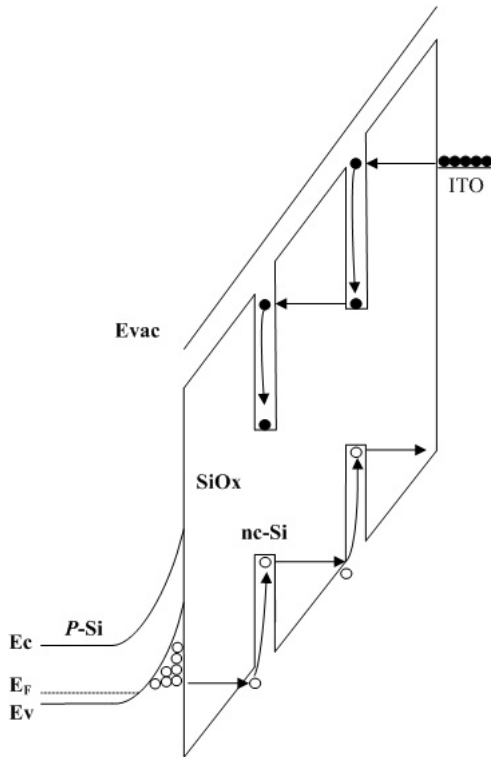


Figure 5. Band diagram of the positively biased ITO/SiO<sub>x</sub>/p-Si MOSLED.

the thermionic tunneling models for a conventional metal–semiconductor junction diode [15], the MOSLED only exhibits direct and Fowler–Nordheim tunneling currents which are not temperature-dependent. When the applied voltage on a MOS diode is smaller than the barrier height of the metal–oxide interface, the electrons have to penetrate through the whole oxide and the gate current is due to direct tunneling in this case. The direct tunneling process will not be involved in a MOS diode with relatively thick oxide film ( $\gg 5$  nm). Because of the existence of a thick oxide layer in the MOSLED, it is further concluded from the above analysis that the only possible carrier transport in the nc-Si based MOSLED is the F–N tunneling process. Without Si nanocrystals, the tunneling current obtained from the pure SiO<sub>2</sub> sample is much lower than that from the PECVD-grown SiO<sub>x</sub> sample. The F–N tunneling threshold electric field is significantly decreased with increasing temperature, corresponding to a reducing metal–oxide barrier height with increasing Si nanocrystal density (see figure 6). By increasing deposition temperature during low-plasma-power PECVD growth, the Si excess condition can be more pronounced as the oxygen decomposition is almost prohibited. Such a specific growth condition further facilitates the reduction of the effective potential barrier height at the ITO–SiO<sub>x</sub> interface. In addition, the temperature dependence of the F–N tunneling current in a MOS structure is described by [15, 16]

$$J_{F-N}(T) = \frac{4\pi q m_{Si} kT}{h^3} \int_{-\infty}^0 \ln \left[ 1 + \exp \left( \frac{E_F - E}{kT} \right) \right] \times \exp \left( -\frac{4\sqrt{2} m_{ox} (-E)^{3/2}}{3\hbar q F} \right) dE, \quad (1)$$

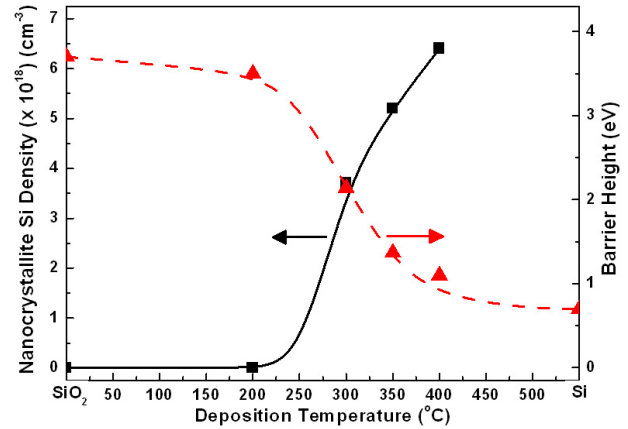


Figure 6. Density of Si nanocrystals in SiO<sub>x</sub> and the effective barrier height at the ITO/SiO<sub>x</sub> interface as a function of deposition temperature.

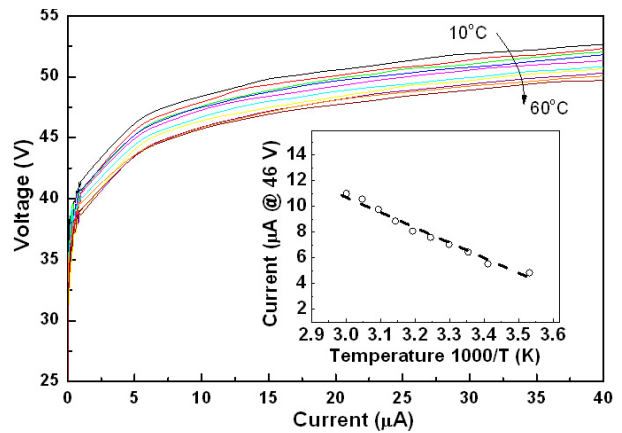
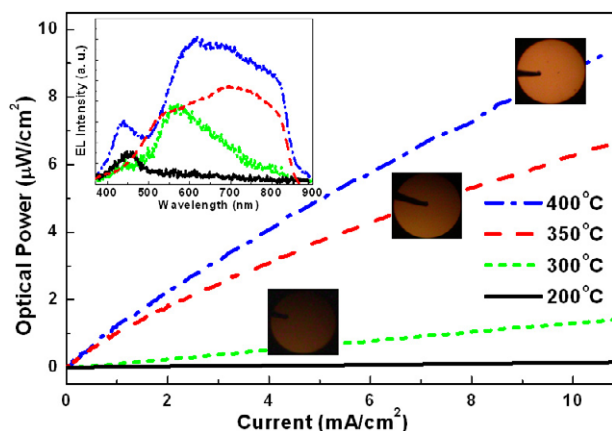


Figure 7. Temperature dependent F–N tunneling characteristics. Inset: Arrhenius plot of temperature dependent current for the MOSLED biased at F–N tunneling threshold.

where  $q$  is the absolute electron charge,  $m_{Si}$  and  $m_{ox}$  are the effective electron mass into the Si and SiO<sub>2</sub>, respectively,  $kT$  is the thermal energy,  $h(\hbar)$  is the (reduced) Planck constant,  $F$  is the electric field across the insulator, and  $E_F$  is the Fermi level. In our experiment, the forward bias current–voltage characteristics of an ITO/SiO<sub>x</sub>/p-Si/Al MOSLED are measured at different temperatures from 10 to 60 °C and shown in figure 7. The inset figure indicates the current of the MOSLED biased at a F–N tunneling threshold of 46 V as a function of  $1000/T$ . The temperature dependent current analysis gives rise to a thermal activation energy of 0.8 eV for initiating the F–N tunneling process in the MOSLED.

It is worth discussing the effect of the environmental oxidation process on the Si-rich SiO<sub>x</sub> film after growth. Within 5 min after growth, the Si-rich SiO<sub>x</sub> samples are moved from the PECVD chamber to a hermetically sealed quartz furnace and annealed in the environment with flowing 99.99% dry N<sub>2</sub> gas. Although the samples are short-term exposed in atmosphere, the maximum oxygen penetration depth is only about 3–5 nm in atmosphere for up to 4 h at room temperature. It is thus difficult to oxidize the individual or clustered Si atoms in the Si-rich SiO<sub>x</sub> film and the oxygen



**Figure 8.** Spectrum, power, and emission patterns of ITO/SiO<sub>x</sub>/p-Si/Al MOSLEDs made on low-plasma PECVD grown Si-rich SiO<sub>x</sub> at different substrate temperatures. Inset: corresponding EL spectra.

atoms in ambient air are difficult to diffuse into the whole Si-rich SiO<sub>x</sub> film in such a short duration. Even though the SiO<sub>x</sub> samples are long-term exposed in atmosphere prior to the RBS diagnosis, different O/Si composition ratios can still be distinguished from among different samples, as proved in figure 4. This analysis also elucidates the minor influence of the room-temperature oxidation effect on the SiO<sub>x</sub> samples. The RBS results are in relatively good agreement with the evidence obtained from EELS analysis shown in figure 4. Moreover, the O/Si composition ratio of the low-temperature PECVD-grown SiO<sub>x</sub> film becomes more stoichiometric than those grown at higher substrate temperature. The enhanced near-infrared EL spectra of the MOSLEDs with increasing deposition temperature are shown in figure 8. The EL is absent in the low-temperature PECVD grown SiO<sub>x</sub> sample since it is unable to provide sufficient Si nanocrystals at PECVD below 200 °C. The oxygen bond and NOV defect related blue-green EL reveal that stoichiometric SiO<sub>2</sub> is grown at a deposition temperature of 200 °C or lower [17]. According to the evidence of EELS and RBS analyses shown in figures 2 and 3, the O/Si composition ratio of the PECVD-grown SiO<sub>x</sub> film at substrate temperature of 200 °C is more stoichiometric (i.e.  $x$  is very close to 2) than those grown at higher substrate temperature. Larger EL power and broader near-infrared spectrum can be obtained from the MOSLEDs made on SiO<sub>x</sub> deposited at higher deposition temperatures [18], since high-temperature deposition introduces excessive Si atoms and a wider Si nanocrystal size distribution. The appearance of NOV related EL strongly correlates with the oxygen deficiency in low-plasma and high-temperature PECVD grown Si-rich SiO<sub>x</sub>, which indicates the strongly oxygen-deficient environment of the SiO<sub>x</sub> matrix, in which the stoichiometry of the SiO<sub>x</sub> film is hard to recovery through post-annealing. This facilitates the low-plasma PECVD grown SiO<sub>x</sub> from remaining in its Si-rich condition even after the high-temperature annealing procedure.

#### 4. Conclusions

The deposition-temperature dependent carrier tunneling and light emission of the Si-rich SiO<sub>x</sub> films grown under low-

plasma-power PECVD has been investigated. Under low-plasma conditions, the oxygen atoms become more deficient to promote dense Si nanocrystals as well as high luminescent efficiency at high substrate temperature, as proved by the decreasing of Si-L<sub>2,3</sub> transition related kinetic energy loss of the primary electrons. In low-plasma and high-temperature deposited samples, the threshold F-N tunneling field and the ITO-SiO<sub>x</sub> junction potential barrier height of ITO/SiO<sub>x</sub>/p-Si/Al MOSLEDs are concurrently reduced due to the increasing Si nanocrystal density. Fewer oxygen atoms can be dissociated from N<sub>2</sub>O and adsorbed on the Si substrate under low-plasma-power and high-temperature deposition. The stronger EL at 455 nm represents the increasing oxygen vacancies during high-temperature deposition as oxygen atoms can hardly adsorb on the substrate. Such a specific growth eventually contributes to an increasing density of excess Si atoms in SiO<sub>x</sub> film, as confirmed by the higher peak intensity, narrower spectral linewidth, and lower kinetic energy loss in EELS analysis. The EL intensity and efficiency of the Si-rich SiO<sub>x</sub> MOSLED is almost 10-fold improved by increasing deposition temperature during the low-plasma-power PECVD growth.

#### Acknowledgments

This work was supported in part by the National Science Council (NSC) of the Republic of China under grants NSC96-2221-E-002-448, NSC96-2221-E-009-282, NSC96-2752-E-229-007-PAE and NSC96-2752-E009-007-PAE.

#### References

- [1] Pavesi L, Dal Negro L, Mazzoleni C, Franzo G and Priolo F 2000 *Nature* **408** 440
- [2] Kalache B, Kosarev A I, Vanderhaghen R and Roca i Cabarrocas P 2003 *J. Appl. Phys.* **93** 1262
- [3] Kondo M, Fukawa M, Guo L and Matsuda A 2000 *J. Non-Cryst. Solids* **266–269** 84
- [4] Lin G-R and Lin C J 2004 *J. Appl. Phys.* **95** 8482
- [5] Lin C J and Lin G-R 2005 *IEEE J. Quantum Electron.* **41** 441
- [6] Cleland T A and Hess D W 1989 *J. Electrochem. Soc.* **136** 3103
- [7] Bauer S H and Haberman J A 1978 *IEEE J. Quantum Electron.* **14** 233
- [8] Schroder D K 1998 *Semiconductor Material and Device Characterization* 2nd edn (New York: Wiley)
- [9] Muttia P, Ghislotti G, Bertoni S, Bonoldi L, Cerofolini G F, Meda L, Grilli E and Guzzi M 1995 *Appl. Phys. Lett.* **66** 851
- [10] Skuja L 1998 *J. Non-Cryst. Solids* **239** 16
- [11] Hren J J, Goldstein J I and Joy D C 1979 *Introduction to Analytical Electron Microscopy* (New York: Plenum)
- [12] Lenzlinger M and Snow E H 1969 *J. Appl. Phys.* **40** 278
- [13] Fowler R H and Nordheim L W 1928 *Proc. R. Soc. A* **119** 173
- [14] Pananakakis G, Ghibaudo G, Kies R and Papadas C 1995 *J. Appl. Phys.* **78** 2635
- [15] O'Dwyer J J 1973 *The Theory of Electrical Conduction and Breakdown in Solids Dielectrics* (Oxford: Clarendon)
- [16] Lu T Z, Alexe M, Scholz R, Talelaev V and Zacharias M 2005 *Appl. Phys. Lett.* **87** 202110
- [17] Lin G-R, Lin C J, Lin C K, Chou L J and Chueh Y L 2005 *J. Appl. Phys.* **97** 094306
- [18] Lin C J, Lee C K, Diao Eric W-G and Lin G-R 2006 *J. Electrochem. Soc.* **153** E25